



**Titre:** Shear strength of angular granular materials with size and shape  
Title: polydispersity

**Auteurs:** Sergio Carrasco, David Cantor, Carlos Ovalle, & Paula Quiroz-Rojo  
Authors:

**Date:** 2023

**Type:** Article de revue / Article

**Référence:** Carrasco, S., Cantor, D., Ovalle, C., & Quiroz-Rojo, P. (2023). Shear strength of angular granular materials with size and shape polydispersity. Open Geomechanics, 4, 1-14. <https://doi.org/10.5802/ogeo.15>  
Citation:

 **Document en libre accès dans PolyPublie**  
Open Access document in PolyPublie

**URL de PolyPublie:** <https://publications.polymtl.ca/55978/>  
PolyPublie URL:

**Version:** Version officielle de l'éditeur / Published version  
Révisé par les pairs / Refereed

**Conditions d'utilisation:** CC BY-NC-SA  
Terms of Use:

 **Document publié chez l'éditeur officiel**  
Document issued by the official publisher

**Titre de la revue:** Open Geomechanics (vol. 4)  
Journal Title:

**Maison d'édition:** Cellule MathDoc/CEDRAM  
Publisher:

**URL officiel:** <https://doi.org/10.5802/ogeo.15>  
Official URL:

**Mention légale:**  
Legal notice:



# OPEN GEOMECHANICS

**Published**

5th September 2023

<https://doi.org/10.5802/ogeo.15>

**Edited by**

Eleni Gerolymatou  
Geomechanics & multiphysics Systems  
Technische Universität Clausthal  
Clausthal, Germany



**Reviewed by**

Vasileios Angelidakis  
Institute for Multiscale Simulation  
Friedrich-Alexander-Universität  
Erlangen-Nürnberg  
Erlangen, Germany  
Debdeep Sarkar  
GuD Geotechnik und Dynamik Consult  
GmbH  
Berlin, Germany  
Francois Guillard  
School of Civil Engineering  
The University of Sydney  
NSW 2006, Australia

**Correspondence**

Carlos Ovalle  
[carlos.ovalle@polymtl.ca](mailto:carlos.ovalle@polymtl.ca)  
Department of Civil, Geological and  
Mining Engineering, Polytechnique  
Montréal, Québec, Canada  
2500 Chem. de Polytechnique  
Montréal, QC H3T 1J4, Canada  
Research Institute of Mining and  
Environment (RIME),  
UQAT-Polytechnique, Québec, Canada

## Shear strength of angular granular materials with size and shape polydispersity

Sergio Carrasco  <sup>a, b</sup>, David Cantor  <sup>a, b</sup>,  
Carlos Ovalle  <sup>a, b</sup> & Paula Quiroz-Rojo  <sup>a, b, c</sup>

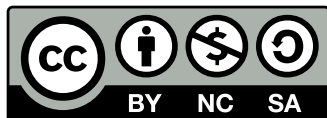
<sup>a</sup> Department of Civil, Geological and Mining Engineering, Polytechnique Montréal, Québec, Canada

<sup>b</sup> Research Institute of Mining and Environment (RIME), UQAT-Polytechnique, Québec, Canada

<sup>c</sup> LMGC, Université de Montpellier, CNRS, Montpellier, France.

**Abstract.** Shear strength characterization of coarse granular materials often requires modifying the original material in order to fit samples in standard testing devices. This is done, however, at the expense of changing the particle size distribution (psd), employing scaling-down techniques such as parallel grading or scalping methods. Such procedures hide, nevertheless, another challenge. As a given particle size can present a characteristic grain shape, altering the grain size distribution can strongly modify the distribution of grain shapes. While the effects of grain shape on shear strength have been vastly covered in the literature, the effect of having different shapes along grain sizes has yet to be systematically assessed and understood. This article explores the critical shear strength of samples composed of particles with size-shape correlations using 2D discrete element simulations. Two cases of particle shape variability across grain sizes are studied: (1) the sharpness of grains' corners - modeled via the number of sides of regular polygons - and (2) the geometric irregularity of grains - where the corners of a polygon are not necessarily evenly spaced. The effects of these geometrical properties on the shear strength are assessed through a series of numerical simple shearing tests up to large levels of deformation. We find that granular materials presenting different number of sides across grain sizes can strongly modify their mechanical response depending on the grain-size correlation. On the contrary, grain shape irregularity turns out not to have a major effect on the critical shear strength. Microstructural analyses allow us to identify how each correlation affects load transmission mechanisms between grains, and the contribution of each grain shape class to the macroscopic shear strength. This work shows that particle sizes are not the only sample descriptor to consider when applying scaling-down techniques. It is equally key to characterize particle shapes across grain sizes to capture the material's mechanical response adequately.

**Keywords.** shear strength, particle shape, polydispersity, discrete-element modeling, grain size distribution



This article is licensed under the Creative Commons Attribution NonCommercial ShareAlike 4.0 License.



Open Geomechanics is member of the Centre Mersenne for Open Scientific Publishing

# 1. Introduction

Stability analyses of earth fills composed of coarse granular materials, such as rockfill dams, mine waste rock dumps, railway ballast, or gravel dikes, require to characterize the shear strength properties of oversized particles that often do not fit in laboratory devices [Bard et al., 2011, Barton and Kjærnsli, 1981, Indraratna et al., 1998, Marachi et al., 1972, Marsal, 1967, Matsuoka et al., 2001, Ovalle et al., 2020]. In such cases, small-scaled samples using scalping or parallel grading techniques are usually prepared to carry out shearing tests [Frossard et al., 2013, Hu et al., 2011, Marachi et al., 1972, Verdugo and de La Hoz, 2007]. Although numerous research has been reported about the effect of these techniques on the shear strength of granular materials, the results widely vary up to the point of being contradictory. While some studies have indicated that shear strength decreases with grain size [Marachi et al., 1972, Ovalle et al., 2014, Varadarajan et al., 2003, Xiao et al., 2014, Zeller and Wullimann, 1957], others have shown the opposite behavior [Al-Hussaini, 1983, Cao et al., 2020, Deiminiat and Li, 2022, Linero et al., 2007]. The sources of this apparent contradiction are presumably found in several sample and testing characteristics, and inherent material properties.

Firstly, concerning sample and testing characteristics, comparing different materials is challenging since neither clear standards have been formulated to assess the relative density of oversized materials nor have authors systematically reported whether their samples are prepared in dense or loose conditions. Therefore, some studies might have used dense samples and reported the peak strength, while others might have tested loose materials and obtained the critical strength. Moreover, using the relative density as a basis for shear strength comparison is not the most appropriate because different particle size distribution (psd) have different density limits [Youd et al., 1973, Zheng and Hryciw, 2016]. In addition, materials can undergo grain crushing at certain stress levels depending on their particle strength, which implies lower dilatancy and, thus, a reduced peak strength [Hardin, 1985, Lade et al., 1996, Ovalle et al., 2015]. Finally, the aspect ratio between the maximum particle size and the characteristic sample size, which is known to have a significant impact on the strength [Amirpour Harehdasht et al., 2019, Cerato and Lutenegeger, 2006, Deiminiat et al., 2020].

Secondly, concerning inherent material properties, altering the psd when preparing small-scaled samples might affect the packing density and, consequently, the peak strength. On the other hand, several works have shown that if all the grains have the same characteristic shape and surface roughness, the critical strength does not depend on the psd [Amirpour et al., 2017, Azéma et al., 2017, Cantor et al., 2018, Deng et al., 2021, Li et al., 2013, Linero et al., 2019, Muir Wood and Maeda, 2008, Voivret et al., 2007a, Yang and Luo, 2018]. However, small scaling techniques could also alter the characteristic grain shape of the material, which would strongly affect the critical strength [Altuhafi et al., 2016, Azéma and Radjai, 2010, Cho et al., 2006, Linero et al., 2019, Nguyen et al., 2015, Nougouier-Lehon, 2010, Xiao et al.,

2019]. This phenomenon has been confirmed by recent studies showing that particle shape could be correlated with grain size due to sedimentary lamination or fine foliation induced by metamorphism in some rockfill materials [Kawamoto et al., 2018, Linero et al., 2017, Liu et al., 2022, Ovalle and Dano, 2020]. Shearing tests over those materials have shown significant differences in critical shear strength after applying small-scaling techniques. Therefore, representative small-scaling sample preparation based only on reducing characteristic grain size needs to be revised if the particle shape distribution changes.

The main objective of this paper is to study the effects of grain size-shape correlations and psd on the critical strength of granular materials. This research extends the work of Carrasco et al. [2022], which presented the effect of particle elongation correlated with grain sizes by introducing a comprehensive analysis of the effects of grain angularity and grain geometric irregularity. We use discrete element modeling (DEM) of 2D granular samples over a large range of psd and analyze the results regarding the macromechanical behavior under critical state conditions. We also isolate the contribution of each family of grain shape and size to the total shear strength, allowing us to describe and understand the effect of particle characteristics on the critical strength.

Is there any particular granulometric class that mainly backs up the macroscopic shear strength? Are grains with sharper corners allowing samples to develop more shear strength independently of their size? What are the main grain geometrical characteristics controlling shear strength that scaling methods should rely on? This research aims to shed light on this set of questions.

## 2. Model material and numerical simulation

We create 2D numerical samples in which grain sizes vary widely from mono-size to highly polydisperse configurations. As grain sizes vary, we also consider two cases of grain shape-size correlations detailed in the following.

### 2.1. Grain shape size correlations

#### Case 1

In this case, we consider grains whose corners can be more or less sharp, being able to develop, respectively, more or less shear strength as shown in the literature [Azéma et al., 2012, Estrada et al., 2011]. This is achieved by varying the number of sides  $n_s$  of regular polygons. This parameter is lower bound to 3, which corresponds to a regular triangle, and as  $n_s$  increases, polygons gradually approach the shape of a disk. We choose to vary  $n_s$  in the range [3,64] as shown in Figure 1, giving us the possibility to explore two different size-shape correlations:

- **Case 1A:** large grains have large  $n_s$  while small have sharper corners.
- **Case 1B:** large grains have sharper corners while small ones have large  $n_s$ .

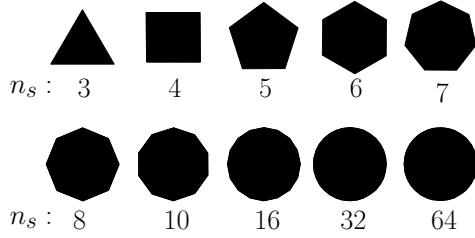


**Figure 1.** Scheme presenting the evolution of corner sharpness, being  $n_s$  the number of sides of regular polygons.

## Case 2

In the second case, we explore another component of grain geometries: shape irregularity of a polygon ( $n_s = 5$ ). While the vertices are evenly separated for a regular polygon, we can model geometries in which the vertices' separation varies as a function of a level of irregularity, as proposed by Nguyen et al. [2015]. We choose to use pentagons for this part of the study since numerous numerical studies have reported their characterization using DEM simulations for mono-size pentagon assemblies [Estrada et al., 2011, Nguyen et al., 2015], providing a reference point for our simulations. For a regular pentagon, the angular position of each vertex can be defined by  $\theta^k = \theta_0 + 2k\pi/5$ , where  $\theta_0$  is the position of the first vertex from the horizontal, and  $k$  is an integer varying from 1 to 5. We can alternatively modify the geometry of the regular pentagon by changing the angular position of vertices  $k$  as:

$$\theta^k = \theta_0 + k \frac{2\pi}{5} \pm \frac{\pi}{5} r_{[0,\delta]}, \quad (1)$$

being  $r_{[0,\delta]}$  a random variable in the range  $[0, \delta]$ ,  $\delta$  is the degree of irregularity that can vary from 0 to 1, and the  $\pm$  sign is randomly chosen for each vertex; see Figure 2.

Similarly to case 1, the geometrical irregularity of pentagonal grains can be studied in two opposite situations:

- **Case 2A:** large grains are irregular pentagons while small ones are regular.
- **Case 2B:** large grains are regular pentagons while small ones are irregular.

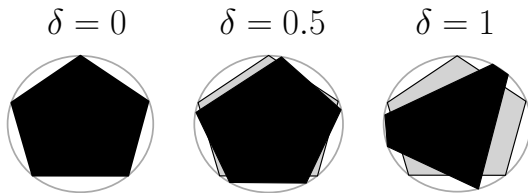


**Figure 2.** Scheme presenting the evolution of grain geometric irregularity as a function of parameter  $\delta$ , based on Nguyen et al. [2015]

## 2.2. Granular sample generation

The construction of numerical samples needs the following procedure:

- the maximum circumscribing particle diameter  $d_{\max} = 15$  mm is defined for all the simulations (note that a polygonal grain size is defined by the diameter of the circle that circumscribes the polygon),
- the number of samples is fixed using the grain size span  $S$  (defined in Eq. 2) varying from 0 (monodisperse sample) to 0.9 (highly polydisperse sample) in steps of 0.1 (i.e., ten different samples per case),

$$S = \frac{d_{\max} - d_{\min}}{d_{\max} + d_{\min}}, \quad (2)$$

- minimal particle size  $d_{\min}$  is calculated by means of  $S$  for each sample,
- the range  $d_{\min}$  to  $d_{\max}$  is discretized in  $N_f = 10$  particle sizes and a uniform psd is set. This means that the surface of a given particle size class is constant for all sizes, resulting in the psd shown in Figure 3,
- depending on the size-shape correlation (i.e., Case 1 or 2), we are able to find the corresponding shape for each particle of size  $d$ .

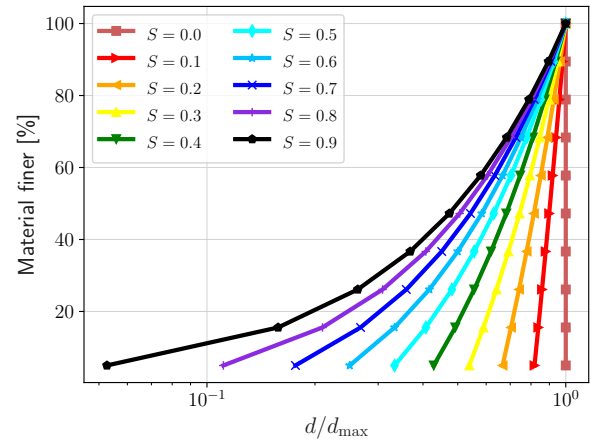


**Figure 3.** Particle size distribution as a function of particle size span  $S$ , where each particle diameter  $d$  is normalized by the maximum particle diameter  $d_{\max}$ .

The last step of the procedure is performed using the following set of rules:

- For Case 1, one of the shapes in the set  $n_s \in [3, 4, 5, 6, 7, 8, 10, 16, 32, 64]$  is assigned to each grain size.
- For Case 2, the following equations characterize the level of irregularity as a function of the relative grain diameter in the assembly  $d_r$ , defined as:

$$d_r = \frac{d - d_{\min}}{d_{\max} - d_{\min}}. \quad (3)$$

Note that this reduced diameter varies between 0 and 1, as the grain belongs to either the smaller or larger classes of particles in the assembly. When the large grains are the most irregular ones the irregularity is equal to  $\delta(d) = d_r$  (Case 2A), and when the large grains are the most regular ones,  $\delta(d) = 1 - d_r$  (Case 2B).

Finally, Figure 4 shows the significant advantage of this generation routine which allows creating assemblies with the same psd, yet the particle shape for each grain size varies significantly. In terms of Wadell's circularity, defined as  $\phi_w = c/C$ , being  $c$  the perimeter of a circle of the same area as the plane figure, and  $C$  is the actual perimeter of the plane figure [Wadell, 1933], Case 1 shows  $\phi_w$  evolving from 0.77 for triangles to 0.99 for polygons with 64 sides. In Case 2,  $\phi_w$  varies from 0.93 for regular pentagons to  $\sim 0.905$  for the most irregular pentagon. To complement the description of psd, we compared the grain size span parameter  $S$ , with the  $D_{50}$ , the uniformity coefficient ( $C_u = D_{60}/D_{10}$ ), and the ratio between the maximum to minimum particle sizes ( $R_D = d_{\max}/d_{\min}$ ). These parameters are presented in Table 1 below.

**Table 1.** Parameters  $d_{\max}$ ,  $d_{\min}$ ,  $R_D$ ,  $D_{50}$  and  $C_u$  for different values of  $S$ .

$S$	$d_{\max}$ [mm]	$d_{\min}$ [mm]	$R_D$	$D_{50}$ [mm]	$C_u$
0	15.0	15.0	1.0	15.0	1.0
0.1	15.0	12.3	1.2	13.7	1.1
0.2	15.0	10.0	1.5	12.5	1.2
0.3	15.0	8.1	1.9	11.5	1.4
0.4	15.0	6.4	2.3	10.7	1.6
0.5	15.0	5.0	3.0	10.0	1.8
0.6	15.0	3.8	4.0	9.4	2.2
0.7	15.0	2.7	5.7	8.8	2.6
0.8	15.0	1.7	9.0	8.3	3.2
0.9	15.0	0.8	19.0	7.9	4.2

### 2.3. DEM simulation

The numerical samples are tested in order to characterize their shear strength properties using a discrete element method known as contact dynamics (CD). The CD method is an approach capable of simulating collections of rigid bodies interacting with frictional contacts. This strategy uses a non-smooth definition of contact laws, which is ideal for dealing with bodies of varied shapes without the need to define stiffness or damping parameters at the variety of contacts that can occur between bodies. In Figure 5, we can notice that in the case of polygons in contact, two different types of interactions can occur: (1) side-vertex ( $sv$ ) and (2) side-side ( $ss$ ). A  $sv$  contact is a single corner of a polygon contacting a side of a neighboring particle. A  $ss$  contact between two rigid polygons can be defined by two point contacts on the common side representing the tangential line [Saussine et al., 2006]. Despite this numerical treatment of a  $ss$  contact, the choice of their loci is inconsequential and only the sum of the two contact forces has a mechanical sense. For more information about the mathematical framework and numerical implementation of the CD method, see references [Dubois et al., 2018, Jean and Moreau, 1992, Moreau, 1988, Radjai and Richefeu, 2009].

Each numerical sample is built with  $N_p \approx 10\,000$  particles, which are placed layer-by-layer in boxes by mean of a potential energy deposition protocol as described

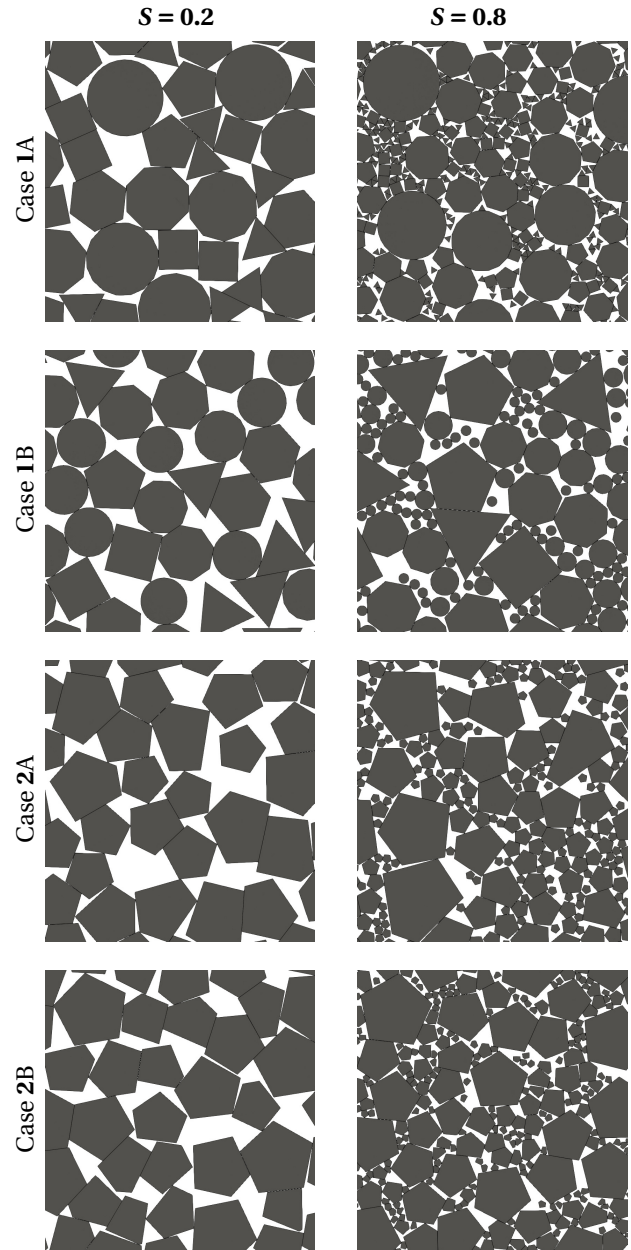


**Figure 4.** Screenshots of samples with particle size span  $S=0.2$  (left) and  $S=0.8$  (right) for different size-shape correlation studies.

in Ref. [Jullien et al., 1992, Visscher and Bolsterli, 1972, Voivret et al., 2007b]. This approach is an efficient strategy to achieve relatively dense random packing configurations without the need of time consuming dynamic simulations. The samples are initially compressed using an isotropic pressure  $P = 10$  kPa using rigid walls around the grain assembly up to a stable solid fraction  $v = A_s/A$ , where  $A_s$  is the total surface area of grains and  $A$  the containing box area. Moreover, all our tests ensured that the sample height ( $h_0$ ) respects the ratio  $h_0/d_{\max} > 10$  to avoid size effects on the mechanical behavior [ASTM, D6528-17, Cerato and Lutenegeger, 2006, Schuhmacher, 2016].

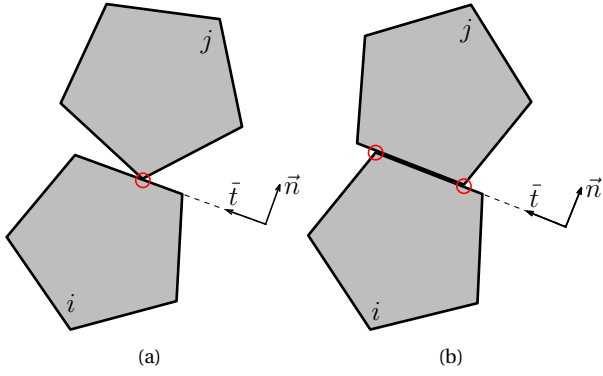


**Figure 5.** Scheme of (a) side-vertex and (b) side-side contacts between two grains labeled  $i$  and  $j$ , where the red circles represent the contact points.

As shown in Figure 6, simple shearing tests are performed by moving the upper and lower wall along axis ‘ $x$ ’ at constant velocity  $v$ , while applying vertical pressure  $P$  along axis ‘ $y$ ’. We set up the shear velocity  $v$  to apply a quasi-static shearing by imposing an inertial number  $I = \dot{\gamma} \langle d \rangle \sqrt{\rho/P} \ll 1$  [GDR-MiDi, 2004], where  $\dot{\gamma} = v/h$ ,  $h$  the height of the sample,  $\langle d \rangle$  is the average particle circumdiameter, and  $\rho$  the grains’ density. The value of the inertial number was set to  $I = 1 \times 10^{-3}$  for all the tests.

In order to reach critical state in terms of macroscopic and microscopic descriptors, we sheared our samples up to a cumulated shear strain  $\gamma = \delta_x/h = 400\%$ , being  $\delta_x$  the cumulated horizontal displacement of the walls. This large deformation was reached by employing periodic boundary conditions along the shearing direction, which allows any particle or contact crossing the periodic boundary to reappear on the sample’s opposite side (see Figure 6). To effectively apply the shearing deformation, we set all particles in contact with the upper and lower walls to follow the wall

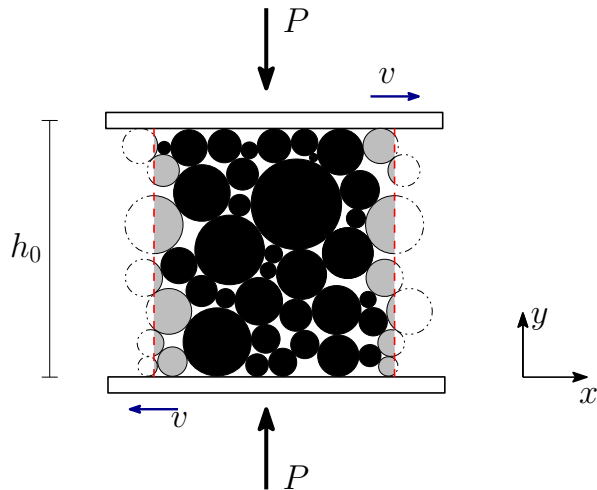


**Figure 6.** Scheme of boundary conditions for the shearing tests. The dashed lines represent the periodic boundary along the  $x$  axis, and the gray particles are the ones under this condition

displacements as if they were ‘glued’ to the boundary, avoiding sliding between grains and walls. For the interactions between grains, the coefficient of friction was set to  $\mu = 0.4$ , and gravity was set to zero to avoid pressure gradients. All shearing tests were performed using the free open-source software LMGC90, capable of simulating discrete mechanical systems in the frame of the CD method [Dubois et al., 2023, 2011].

### 3. Macroscopic behavior

The macroscopic behavior in our tests can be characterized by the solid fraction  $v$  and the normalized shear stress  $q/p$ , being  $q$  the deviatoric stress and  $p$  the mean pressure of the granular stress tensor  $\sigma$ . This tensor is computed using the following expression [Andreotti et al., 2013, Nicot et al., 2013, Rothenburg and Bathurst, 1989]:

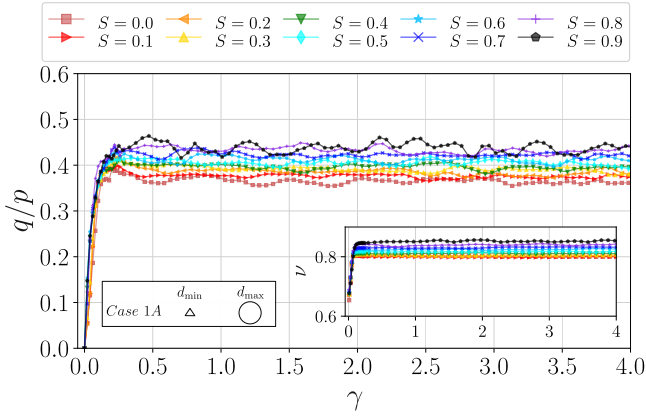
$$\sigma_{ij} = \frac{1}{A} \sum_{\forall c} f_i^c \ell_j^c, \quad (4)$$

where  $f_i^c$  is the  $i$  component of the force at contact  $c$ , and  $\ell_j^c$  is the  $j$  component of the branch vector (i.e., the vector joining the center of mass of touching particles at contacts  $c$ ). We use the principal stresses of  $\sigma$  (i.e.,  $\sigma_1$  and  $\sigma_2$ ) to calculate  $q = (\sigma_1 - \sigma_2)/2$  and  $p = (\sigma_1 + \sigma_2)/2$ . The coefficient of internal friction is given by  $\mu^* = q/p = \sin(\phi)$  at the critical state, being  $\phi$  the macroscopic friction angle of the material.

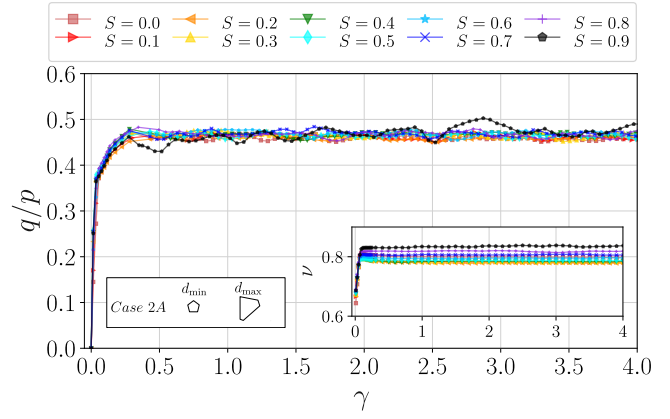
Figures 7 and 8 show the evolution of  $v$  and  $q/p$  for all cases as a function of the shear deformation  $\gamma$ . For the shear stress  $q/p$ , we observe a gradual gain of resistance in all the cases up to  $\gamma \sim 0.2$ . Then, a transient zone towards the steady state takes place that varies depending on the material. While in Case 1A the steady state is reached around  $\gamma \sim 0.4$ , in case 1B the stabilization occurs more rapidly, as soon as  $\gamma \sim 0.3$ . For the Cases 2A and 2B, the shear strength stabilization occurs practically at the same levels of deformation (i.e.,  $\gamma \sim 0.3$ ). In terms of volume of the sample, we observe that in all cases the solid fraction finds steady values earlier than the shear strength, around  $\gamma \sim 0.25$ . Although the critical state is reached before  $\gamma \sim 0.5$ , we decided to shear the samples up to 400% shear deformation to ensure that both macroscopic and microscopic parameters find stable values despite relatively small fluctuations. To characterize the critical state, we average the values for the last 100% of deformation out of the total 400% accumulated.

Figure 9 shows the evolution of the average solid fraction for both cases and all the grain size spans in the critical state. For Cases 1A and 1B (Figure 9(a)), we can observe that solid fraction increases from  $v \approx 0.8$  for  $S = 0$  to  $v \approx 0.85$  for  $S = 0.9$ . Nevertheless, while for Case 1A  $v$  gradually increases with  $S$  as small angular grains can fill voids between larger particles, in Case 1B, the solid fraction presents a parabolic trend with a minimal  $v \approx 0.79$  for  $S = 0.4$ . This evolution in Case 1B might be related to the development of large cavities between larger sharper particles only after  $S > 0.5$ . Despite the difference in size-shape correlation, we obtain a similar value of  $v$  for both cases for  $S = 0.9$ .

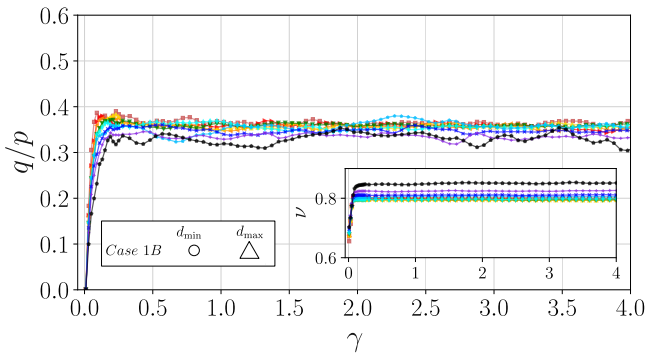
On the other hand, Figure 9(b) shows that Cases 2A and 2B have similar evolutions of  $v$  as grain size span increases,



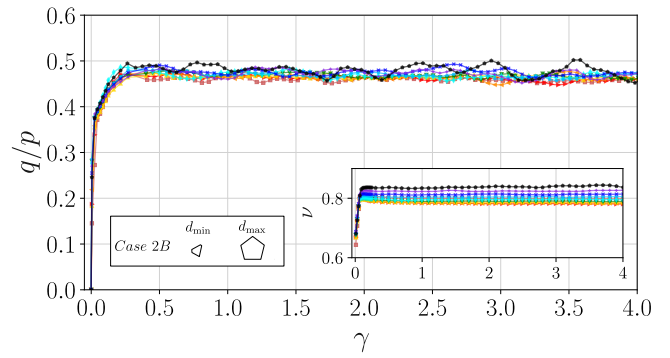
(a)



(a)



(b)



(b)

**Figure 7.** Evolution of shear stress  $q/p$  and solid fraction  $\nu$  (inset) for Cases 1A (a) and 1B (b) as a function of the shear deformation  $\gamma$ .

**Figure 8.** Evolution of shear stress  $q/p$  and solid fraction  $\nu$  (inset) for Cases 2A (a) and 2B (b) as a function of the shear deformation  $\gamma$ .

being Case 2B slightly denser than Case 2A. This suggests that small irregular pentagons can more efficiently fill the voids left by larger regular pentagons.

In terms of critical state shear strength, Figure 10 shows the evolution of the average  $q/p$  for the different size-shape correlations. For assemblies composed of same-shape regular polygons, previous studies have shown that the shear strength varies exponentially as a function of particle sharpness, from  $q/p \approx 0.27$  for disks [Voivret et al., 2007a] to  $q/p \approx 0.47$  for triangles [Estrada et al., 2011]. Effectively, the mean values of  $q/p$  at critical state that we found in Figure 10(a) lay between those extreme cases. For Case 1A, the shear strength increases linearly as  $S$  increases from  $q/p \approx 0.36$  for  $S = 0$  to  $q/p \approx 0.43$  for  $S = 0.9$ , while for Case 1B, the shear strength slightly decreases to  $q/p \approx 0.32$  for  $S = 0.9$ .

Figure 10(b) shows the evolution of the shear strength in the critical state as a function of  $S$  for Cases 2A and 2B. Unexpectedly, both cases show similar trends for  $q/p$ , being slightly higher as the grain size span increases. However, this variation is so small that we can suggest that the shear strength is practically independent of the size-shape correlation. Figure 10(b) also shows values of  $q/p$  for granular assemblies composed of only regular ( $\delta = 0$ ) and irregular pentagons ( $\delta = 1$ ) assemblies, being  $q/p = 0.49$  and

$q/p = 0.46$ , respectively [Estrada et al., 2011, Nguyen et al., 2015]. It is observed that the different results of  $q/p$  in our simulations are within such a range, although slightly closer to the case of irregular particles.

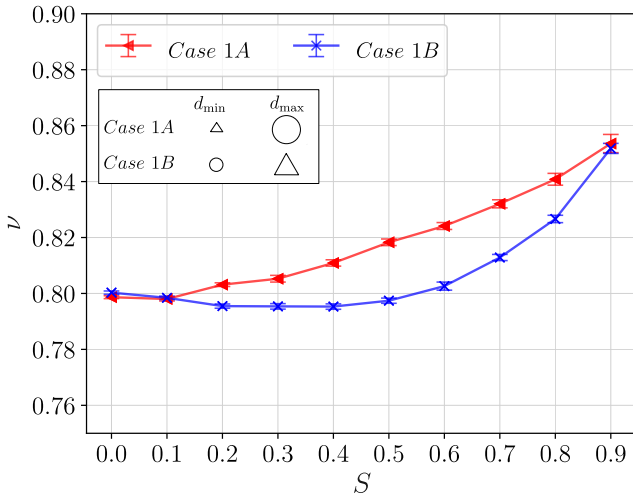
This set of results put in evidence the fact that (1) grain sharpness plays a major role on the macroscopic shearing response and (2) equal particle size distributions may present dramatically different macroscopic behavior (in terms of strength and density) depending on their grain size-shape correlation.

In order to understand the macroscopic effects of each grain shape given its relative size in a sample, it is key to explore micromechanical aspects related to the grain organization and force transmission mechanisms for each of the cases tested.

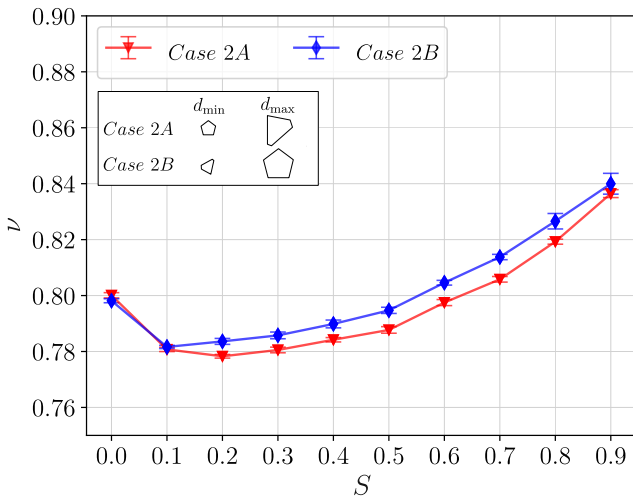
## 4. Microscopic behavior

### 4.1. Connectivity

We can characterize the particle organization using an indicator of their connectivity through the *coordination number* or average number of contacts per load-bearing grain. This parameter is defined as  $Z = 2N_c/N_p^*$ , where  $N_c$  is the total number of force-bearing contacts, and  $N_p^*$  the number



(a)

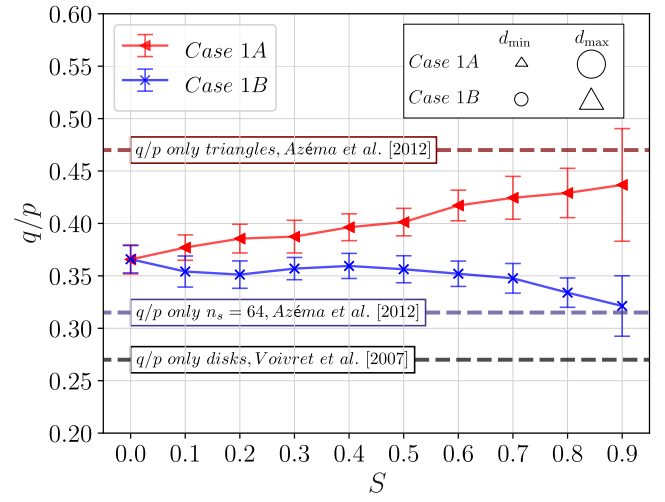


(b)

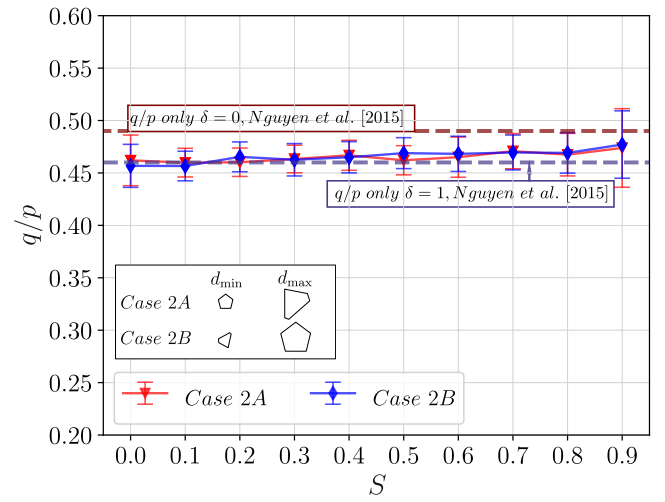
**Figure 9.** Evolution of the average solid fraction  $\nu$  at critical state as a function of the particle size dispersion  $S$  for Case 1 (a) and Case 2 (b). Error bars display the standard deviation of the data.

of grains transmitting forces. The coordination number excludes all particles having less than two active contacts (i.e., floating particles) to compute  $N_p^*$ . In this vein, it is also possible to estimate the proportion of grains not participating in the transmission of forces as  $c_0 = N_p^0/N_p$ , being  $N_p^0$  the number of floating particles and  $N_p$  the total number of particles in the assembly.

Figure 11(a) shows the evolution of  $Z$  and  $c_0$  as a function of  $S$  for Cases 1A and 1B. For mono-shape polygonal assemblies, the coordination number is bounded between  $Z \in [3.1, 3.5]$  [Azéma et al., 2012]. The inclusion of grains with different sharpness affects the connectivity at critical state, allowing the assemblies to have a broader range for  $Z$ . As grain size span increases, Cases 1A and 1B present opposite trends with an increase of  $Z$  for assemblies containing large particles with low sharpness (high  $n_s$ ) (varying from  $Z = 3.6$



(a)

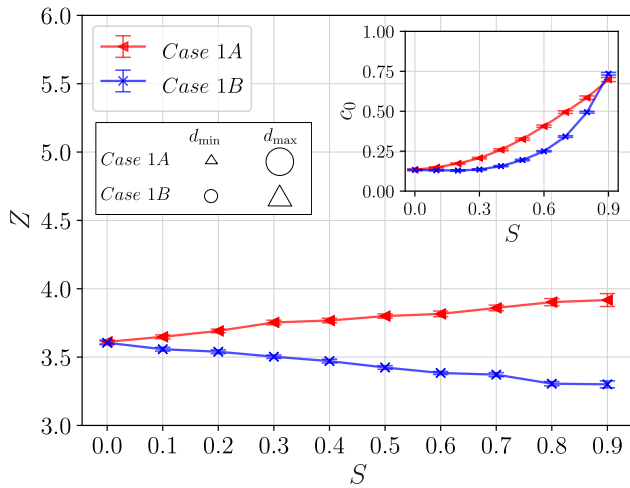


(b)

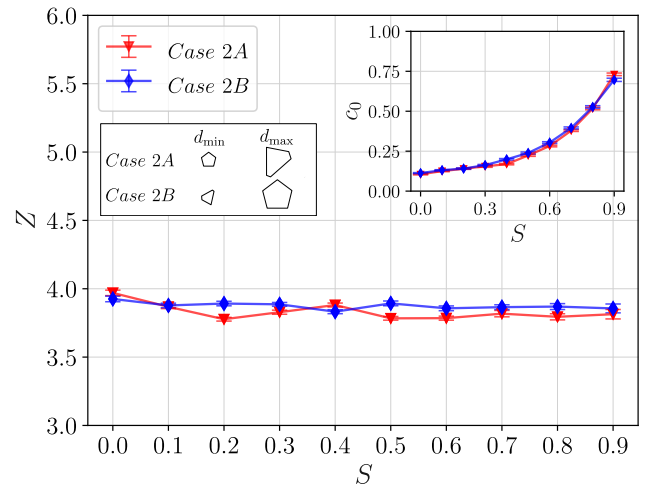
**Figure 10.** Evolution of the average critical shear strength  $q/p$  as a function of the particle size dispersion  $S$  for Case 1 (a) and Case 2 (b). Error bars display the standard deviation of the data.

to 3.9 in Case 1A) and a drop of connectivity as the assembly contains large sharp grains (low  $n_s$ ) (from  $Z = 3.6$  to 3.3 for Case 1B). The inset in the same figure shows the evolution of  $c_0$  as a function of  $S$  for Cases 1A and 1B. In both cases,  $c_0$  gradually increases with  $S$  due to a large proportion of small particles rattling between larger particles; namely,  $c_0$  increases from  $\sim 0.16$  for  $S = 0$  to  $\sim 0.70$  for  $S = 0.9$  for Cases 1A and 1B, respectively. To analyze this behavior in detail, we consider the coordination number by particle family  $Z_f$  (i.e., the average number of contacts per particle of shape  $n_s$  or  $\delta$ ) as a function of  $d_r$ . Figures 11(b) and 11(c) present the average number of contacts  $Z_f$  in Cases 1A and 1B as a function of  $d_r$ . Interestingly, we observe an almost linear dependence between  $Z_f$  and  $d_r$ , with an increasing slope as  $S$  increases. Similar behavior is observed in simulations of spheres and irregular pentagons [Cantor et al., 2018, Nguyen

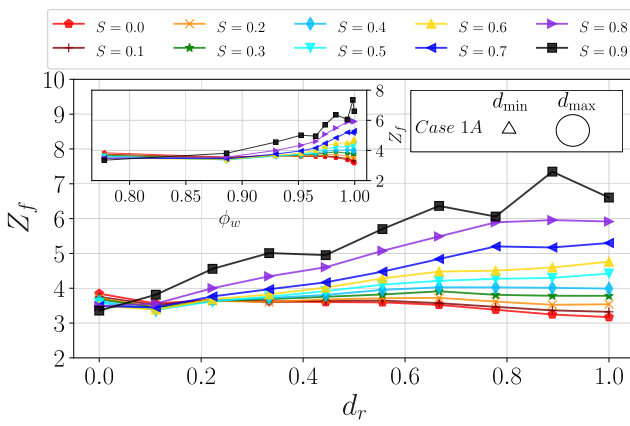




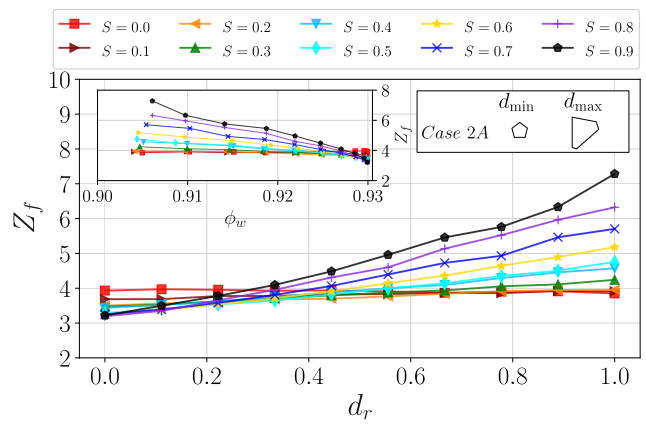
(a)



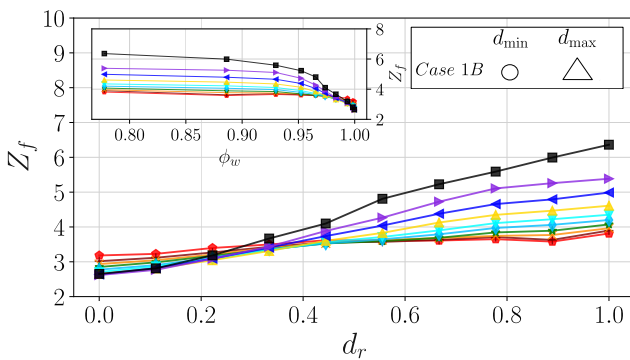
(a)



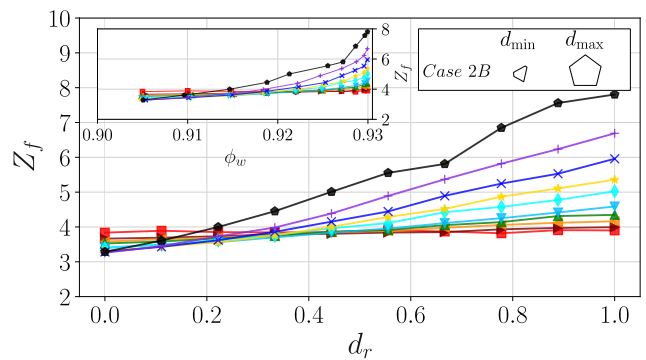
(b)



(b)



(c)



(c)

**Figure 11.** Evolution of  $Z$  at critical state as a function of the particle size dispersion  $S$  and for Cases 1A and 1B (a), and evolution of  $Z_f$  per particle family for Cases 1A (b) and 1B (c) as a function of  $d_r$  and as a function of  $\phi_w$  in the inset figure.

**Figure 12.** Evolution of  $Z$  at critical state as a function of the particle size dispersion  $S$  and for Case 2A and 2B (a), and evolution of  $Z$  per particle family for Case 2A (b) and Case 2B (c) as a function of  $d_r$  and as a function of  $\phi_w$  in the inset figure.

et al., 2015]. These figures confirm that larger particles are always more connected than small ones independently of the grain shape distribution. If we compare  $Z_f$  in inset figures of Cases 1A and 1B, larger particles with high  $n_s$  are always better connected than larger sharper particles, as opposed

to the smaller particles where less circular grains tend to be more connected. This behavior is presumably due to the capacity of small sharper particles to reach neighboring particles with their corners that are normally unreachable for less angular grains Azéma et al. [2012].

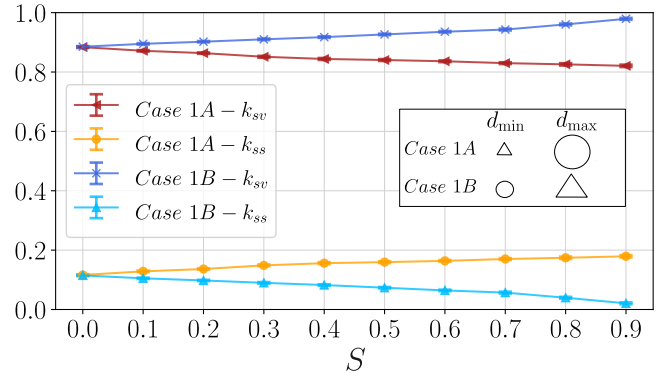
In Figure 12(a), we can observe  $Z$  and  $c_0$  as a function of  $S$  for Cases 2A and 2B. We observe that the connectivity among grains is almost constant with a value of  $Z = 3.8$ , regardless of  $S$ . Both size-shape correlations of irregular to regular pentagons (i.e., Cases 2A and 2B) allow having a better-connected assembly than for only regular pentagons, where  $Z = 3.2$  [Azéma et al., 2012]. Figures 11(b) and 11(c) present the average number of contacts  $Z_f$  in Cases 2A and 2B as a function  $d_r$ . We can observe - as in Cases 1A and 1B - a linear dependence between  $Z_f$  and  $d_r$  that is almost identical in both cases. Comparing both size-shape correlations based on irregularity, we can hardly detect a difference in the microstructural evolution of connectivity. Therefore, the sharpness of the grains in Cases 2A and 2B (i.e., pentagons), instead of their degree of irregularity, seems to be a more meaningful geometric parameter controlling the behavior of these assemblies.

## 4.2. Influence of the type of contact between grains

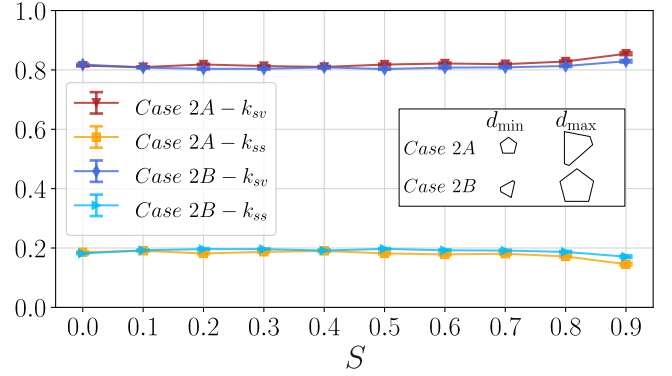
Previous numerical works have shown that contact types between angular grains can play a crucial role in the development of macroscopic strength [Acevedo et al., 2013, Botton et al., 2013, Hidalgo et al., 2009, Kanzaki et al., 2011, Matsushima and Chang, 2011]. For instance, it has been observed that the proportion of side-side contacts in packings of polygons under shearing has an essential role in stress transmission and mobilization of strength for most angular particles. Nevertheless, those results were found in samples containing only grains of the same shape, and it is not clear whether that observation holds up for size-shape correlated grain assemblies.

We study the influence of the side-vertex and side-side contacts in our samples. As shown in Figure 13, we quantify the proportion  $k$  of each type of contact (i.e.,  $k_{ss}$  and  $k_{sv}$ , respectively), as a function of  $S$ . We can observe that the proportion of contacts type evolves in opposite trends for Cases 1A and 1B. As a matter of fact, the number of  $ss$  contacts increases for Case 1A and decreases for Case 1B as the grain size span increases, which agrees with the macroscopic shear strength trends.

Using mono-shape assemblies, Azéma et al. [2012] have shown that  $k_{ss}$  varies exponentially as a function of particle sharpness, from  $k_{ss} \approx 0$  for circles to  $k_{ss} \approx 0.25$  for triangles. Despite the fact that larger grains are always better connected than smaller ones, our results suggest that the capability of granular samples with size-shape correlations to generate  $ss$  contacts is mainly determined by the shape of the classes of small grains. This can be understood considering the fact that there are many more small grains in the sample compared to larger grains, so they can promote a greater numerical proportion of their preferred contact type. To put this in evidence, Figure 14 shows screenshots of the samples at a given instant under critical state for Cases 1A and 1B with  $S = 0.0$  and  $S = 0.8$ ; floating particles are shown in light gray, while grains transmitting forces are shown in black. The lines connecting the centers of touching grains correspond to the contact network and the line thickness is



(a)



(b)

**Figure 13.** Evolution of the proportion of contact type ( $k_{sv}$  and  $k_{ss}$ ) at critical state as a function of the grain size dispersion  $S$  for Cases 1A and 1B (a), and Cases 2A and 2B (b)

proportional to the magnitude of the normal force. The color of the lines also indicates whether it is  $ss$  (green) or  $sv$  (red) contact.

For Cases 2A and 2B, Figure 13(b) shows the proportion of  $k_{sv}$  and  $k_{ss}$  as a function of  $S$ . Both contact proportions remain very similar for all grain size spans and all size-shape correlations, which is consistent with the strength found in such Cases.

While the proportion of number of contacts is of great interest, the effective contribution of each contact type to the macroscopic strength might be slightly different due to the magnitude of forces that each contact carries depending on the size of grains in interaction. To explore the micromechanical contributions of the contact type to the macroscopic shear strength, we can define the stress tensor as a sum of two partial tensors representing the contribution of  $sv$  and  $ss$  contacts. Employing the expression (4) and limiting the sum per contact type as:

$$\sigma_{ij} = \sigma_{ij}^{sv} + \sigma_{ij}^{ss}, \quad (5)$$

where

$$\sigma_{ij}^{sv} = \frac{1}{A} \sum_{\forall c^{sv}} f_i^c \ell_j^c, \quad (6)$$

and

$$\sigma_{ij}^{ss} = \frac{1}{A} \sum_{\forall c^{ss}} f_i^c \ell_j^c, \quad (7)$$

being  $c^{sv}$  and  $c^{ss}$  the corresponding contacts types. Using these partial tensors, we can compute the contribution of each one to the macroscopic strength since  $q = q^{ss} + q^{sv}$ , being  $q^{ss}$  and  $q^{sv}$ , the deviatoric components of each partial tensor. Figure 15 shows the evolution of  $q/p$ ,  $q^{sv}/p$ , and  $q^{ss}/p$  as a function of grain size span  $S$ . For Case 1B, where larger particles are sharper and smaller ones have high  $n_s$ , the contributions of  $sv$  contacts remain constant as  $S$  increases, even though the number of contacts  $k_{sv}$  increases with the size dispersion.

On the other hand, for Case 1A, both contact types increase their contributions to  $q/p$  as  $S$  increases, although it is only  $k_{ss}$  the one that increases as the  $S$  increases.

For Cases 2A and 2B, the evolution of  $q^{sv}/p$  and  $q^{ss}/p$  is practically the same for both cases as  $S$  increases. There are no major differences in the contributions to shear strength, whether the fraction of smaller grains is composed of regular or irregular pentagons. Nonetheless, the contribution to

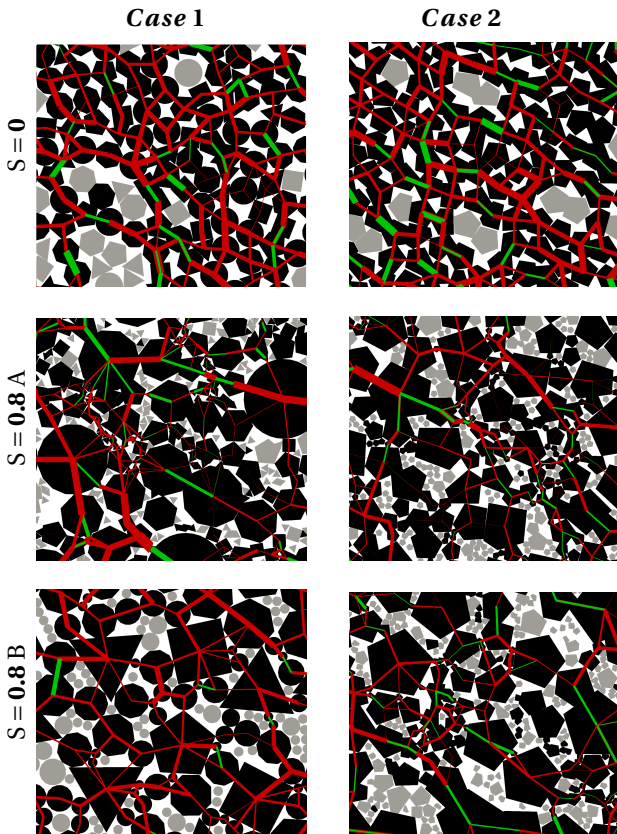
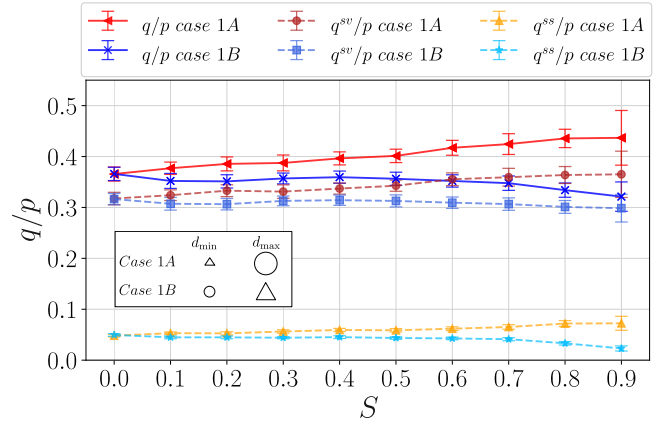
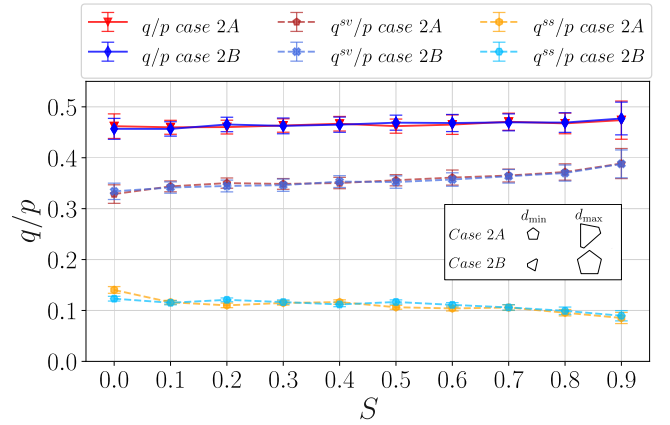


**Figure 14.** Screenshots of samples at critical state for Case 1 (left) and Case 2 (right) for different size span and size-shape correlation. The green and red lines joining the center of mass of touching grains indicate whether it corresponds to a  $ss$  or  $sv$  contact, respectively.



(a)



(b)

**Figure 15.** Decomposition of the deviatoric component of stresses  $q/p$  (at critical state) by contribution of side-vertex  $q^{sv}/p$  and side-side  $q^{ss}/p$  contacts for Cases 1A (a) and 1B (b) as a function of the grain size span  $S$ .

shear strength of  $sv$  contacts increases while that of  $ss$  decreases in similar proportions. This compensation of contributions helps to explain why the macroscopic response  $q/p$  remains practically constant with  $S$ .

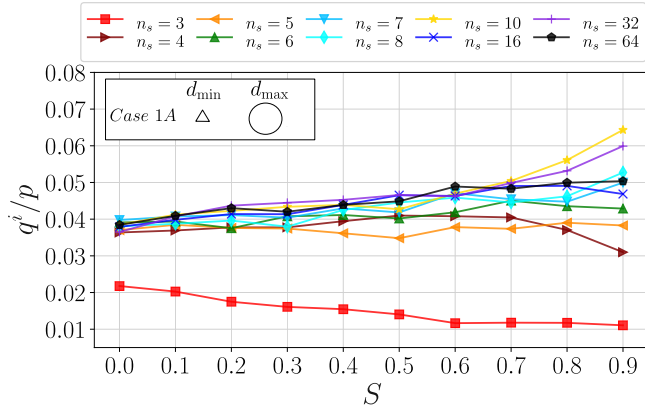
### 4.3. Contributions to shear strength by shape class

We employ an alternative decomposition of  $q/p$  to access the contributions of each shape class on the critical shear strength [Cantor et al., 2020]

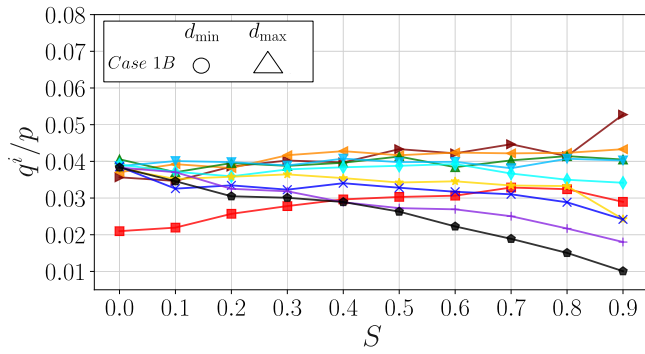
$$\frac{q}{p} = \frac{1}{p} \sum_{i=1}^{N_{sc}} q^i, \quad (8)$$

being  $q^i$  the deviatoric component of the granular stress tensor  $\sigma^i$  for each particle *shape class* ( $sc$ ) in the assembly. This tensor is computed using the following expression:

$$\sigma_{mn}^i = \frac{1}{A} \sum_{\forall N_p^{*i}} f_m^c r_n^c, \quad (9)$$



(a)

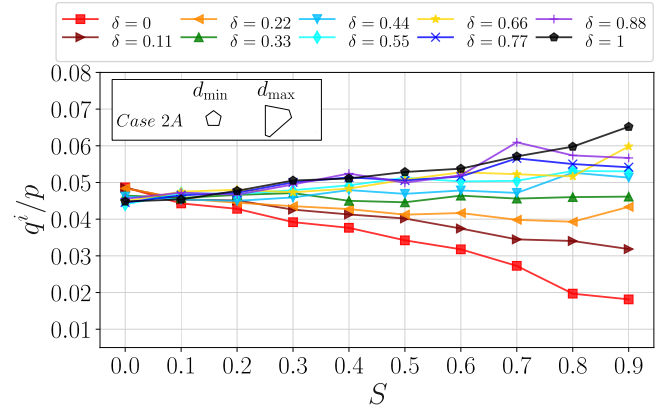


(b)

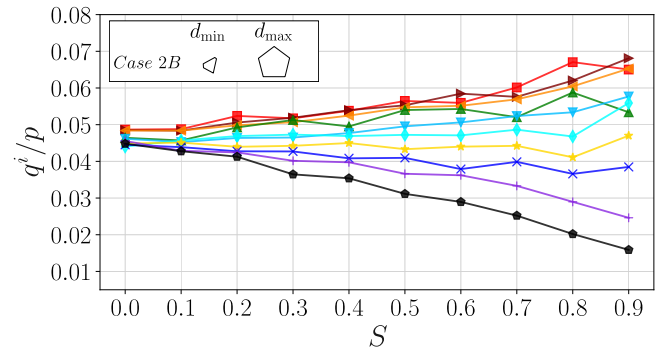
**Figure 16.** Decomposition of the deviatoric component of stresses (at critical state) by shape class for Cases 1A (a) and 1B (b) as a function of the grain size span  $S$ .

where  $N_p^{*i}$  is any load-bearing grain with a given shape ‘ $i$ ’,  $f_m^c$  is the  $m$  component of the force at contact  $c$ , and  $r_n^c$  is the  $n$  component of the vector joining the center of mass of particle and the contact point. We use the principal stresses of  $\sigma^i$  (i.e.,  $\sigma_1^i$  and  $\sigma_2^i$ ) to calculate  $q^i = (\sigma_1^i - \sigma_2^i)/2$  and  $p^i = (\sigma_1^i + \sigma_2^i)/2$  for each family shape. Figure 16 presents the deviatoric contributions by shape classes to  $q/p$  at critical state for size-shape correlations 1A and 1B as a function of  $S$ . Note that the shape classes are separated into ten groups for Cases 1A and 1B as they are categorized by the number of sides of the grains. For mono-size samples  $S = 0$ , we observe that, at critical state, all polygons contribute  $q^i/p$  around 0.35 to 0.40, except for the triangles where  $q^i/p$  is slightly lower. In general, the coarse fractions of the sample increase their contributions to total critical  $q/p$ . This behavior is even more marked as size span  $S$  increases.

For Case 1A, the coarser and less sharp fractions increase their contributions by around 30 – 70% when passing from monodisperse to highly polydisperse samples. For Case 1B, where the coarse fraction is composed of sharper grains, we observe that only the most sharp classes (i.e., triangles and squares) increase their contribution to the global shear strength.



(a)



(b)

**Figure 17.** Decomposition of the deviatoric component of stresses (at critical state) by shape class for Cases 2A (a) and 2A (b) as a function of the grain size span  $S$ .

On the other hand, by studying the evolution of  $q^i/p$  at critical state for the finer fraction of particles, we can observe for Case 1A that square and triangular particles decrease their contribution as  $S$  increases. In particular, the sharpest particles reduce to almost half their contribution to the global shear strength as  $S$  increases. For Case 1B, we observe a significant drop in the contributions to strength of small less sharp grains as  $S$  increases. For instance, 10-side polygons decrease their contribution by almost half, and for 64-side polygons, the drop of about 1/4 when comparing the mono-size and the polydisperse cases.

These curves help to understand that the drop of critical  $q/p$  in Case 1B is mainly due to a significant decrease in shear strength provided by the less sharp grains. In contrast, Case 1A has a generalized increment of critical  $q/p$  because small sharp grains contribute significantly to the shear strength, while larger less sharp grains present slight increments of strength.

Figure 17 shows the evolution of  $q^i/p$  to critical shear strength for Cases 2A and 2B, where the shape class is related to the irregularity of pentagonal grains. We observe an identical evolution of contributions by shape class for both cases. The drop in strength of the finer fraction is fully compensated by the increase in the contribution of the coarse

fraction, regardless of the characteristic grain shape of the finer fraction.

## 5. Conclusion

This paper studied the effects of granular assemblies presenting correlations between the size and the shape of the grains. Two cases covering different shape descriptors were considered and modeled. In the first case, we use regular polygons with two different size-shape correlations: Case 1A, where large grains are less sharp than small ones, and Case 1B, where large grains are sharper than small ones. In the second case, we use pentagons with two different size-shape correlations: Case 2A, where large grains are regular pentagons and small ones are irregular, and Case 1B, where large grains are irregular pentagons and small ones are regular. Our granular assemblies varied from mono-size to polydisperse arrangements of grains where  $d_{\max}/d_{\min} \approx 20$ . Employing the discrete element method known as contact dynamics, we simulated 2D granular assemblies under simple shearing employing periodic quasi-static conditions up to a cumulated shear deformation of  $\gamma = 400\%$ .

We observed that size-shape correlations based on sharpness profoundly modify the mechanical response of the granular assemblies, while grain irregularity in pentagons did not show any significant impact on the mechanical behavior as grain size span is varied.

In systems with size-shape correlation based on grain sharpness, assemblies in Case 1A show that shear strength significantly increases with grain size span. The opposite size-shape correlation, Case 1B, shows a drop in shear strength as the grain size span increases.

To understand the differences between Cases 1A and 1B, we undertook a series of microstructural analyses and showed that each correlation strongly affects the grain connectivity, being the assembly in Case 1A able to develop more contacts per particle on average. Furthermore, we decomposed the connectivity by grain size and observed that the connectivity of larger grains always increases independently of the grain size-shape correlation. Our results also related higher values of  $Z$  with the presence of more side-side contacts, which allows a more stable contact network to be formed.

Finally, we also decomposed the deviatoric component of the shear strength critical  $q/p$  by contributions of different shape classes. This analysis showed that larger grains contribute more to the shear strength as the grain size span increases. This phenomenon is more intense when large grains are less sharp. In turn, the same analysis showed that smaller grains have fewer contributions to the shear strength as the grain size span increases. Specifically, the contribution of smaller particles drops around two times more when their shapes have a large number of sides than when the particles are sharp.

For Cases 2A and 2B, we also decomposed  $q/p$  at critical state by contributions of different shape classes  $q^i/p$ , showing a practically identical evolution of contributions by shape class for both cases, being the largest grains those always contributing more than the small grains. The increase

in the contribution of the coarse fraction is then fully compensated by the drop in resistance of the finer fraction. Consequently, there is no difference in whether the finer fraction is regular or irregular.

Together with a previous research on the effects of particle size-elongation correlations [Carrasco et al., 2022], this work proves that different grain size-shape correlations can have major effects on the critical shear strength and solid fraction of granular assemblies. These facts suggest that scaling methods based on scalping or parallel psd can imply significant errors when estimating the shear strength of a material in a small-scaled sample if grain shapes are not taken into account in the procedure.

Future studies on this topic should focus on exploring more realistic size-shape correlations seen in geomaterials, as well as include the possibility of grains to break. Another important challenge in this topic concerns the extension and validation of the two-dimensional size-shape correlations to three-dimensional modeling and simulation. The validation of these numerical observations concerning grain shape and size effects through laboratory tests is highly desired but rarely seen in the literature. The challenges of experimental testing to reproduce broad grain size distribution while carefully controlling the grain shape is still an open issue that calls for large-scale testing or alternative physical approaches.

## Conflicts of Interest

The authors declare no conflicts of interest. The complete review history is available online.

## Acknowledgements

This research work benefited from the financial support of the Natural Sciences and Engineering Research Council of Canada (NSERC) [Ref. RGPIN-2019-06118 & ALLRP 571865-21], the Fonds de recherche du Québec — Nature et technologies (FRQNT) through the « Programme de recherche en partenariat sur le développement durable du secteur minier-II » [Ref. 2020-MN-281267], the industrial partners of the Research Institute on Mines and the Environment (RIME) UQAT- Polytechnique (irme.ca/en), Calcul Quebec and Compute Canada Compute Canada through the Resources for Research Groups (RRG) Competition.

## References

- Acevedo, M., Hidalgo, R. C., Zuriguel, I., Maza, D., and Pagonabarraga, I. (2013). Influence of the feeding mechanism on deposits of square particles. *Phys. Rev. E*, 87.
- Al-Hussaini, M. (1983). Effect of particle size and strain conditions on the strength of crushed basalt. *Can. Geotech. J.*, 20(4):706–717.
- Altuhafi, F. N., Coop, M. R., and Georgiannou, V. N. (2016). Effect of Particle Shape on the Mechanical Behavior of Natural Sands. *J. Geotech. Geoenviron.*, 142(12).
- Amirpour, H. S., Karray, M., Hussien, M., and Chekired, M. (2017). Influence of particle size and gradation on

- the stress-dilatancy behavior of granular materials during drained triaxial compression. *Int. J. Geomech.*, 17(9).
- Amirpour Harehdasht, S., Hussien, M. N., Karray, M., Roubtsova, V., and Chekired, M. (2019). Influence of particle size and gradation on shear strength–dilatation relation of granular materials. *Can. Geotech. J.*, 56(2):208–227.
- Andreotti, B., Forterre, Y., and Pouliquen, O. (2013). *Granular media: between fluid and solid*. CUP.
- ASTM, D6528–17 (2017). Standard test method for consolidated undrained direct simple shear testing of fine grain soils. Standard, American Society for Testing and Materials, West Conshohocken, PA.
- Azéma, E., Estrada, N., and Radjai, F. (2012). Nonlinear effects of particle shape angularity in sheared granular media. *Phys. Rev. E*, 86(4).
- Azéma, E., Linero, S., Estrada, N., and Lizcano, A. (2017). Shear strength and microstructure of polydisperse packings: The effect of size span and shape of particle size distribution. *Phys. Rev. E*, 96.
- Azéma, E. and Radjai, F. (2010). Stress-strain behavior and geometrical properties of packings of elongated particles. *Phys. Rev. E*, 81(5).
- Bard, E., Anabalón, M. E., and Campaña, J. (2011). Waste rock behavior at high pressures: dimensioning high waste rock dumps. pages 83–112. Wiley Online Library.
- Barton, N. and Kjærnsli, B. (1981). Shear strength of rockfill. *J. Geotech. Eng.*, 107(7):873–891.
- Boton, M., Azéma, E., Estrada, N., Radjai, F., and Lizcano, A. (2013). Quasistatic rheology and microstructural description of sheared granular materials composed of platy particles. *Phys. Rev. E*, 87.
- Cantor, D., Azéma, E., and Preechawuttipong, I. (2020). Microstructural analysis of sheared polydisperse polyhedral grains. *Phys. Rev. E*, 101.
- Cantor, D., Azéma, E., Sornay, P., and Radjai, F. (2018). Rheology and structure of polydisperse three-dimensional packings of spheres. *Phys. Rev. E*, 98(5).
- Cao, P., Jiang, M., and Ding, Z. (2020). Effects of particle size on mechanical behaviors of calcareous sand under triaxial conditions. *Jpn. Geotech. Soc. spec. publ.*, 8(5):182–187.
- Carrasco, S., Cantor, D., and Ovalle, C. (2022). Effects of particle size-shape correlations on steady shear strength of granular materials: The case of particle elongation. *Int. J. Numer. Anal. Methods. Geomech.*, 46(5):979–1000.
- Cerato, A. B. and Lutenecker, A. J. (2006). Specimen size and scale effects of direct shear box tests of sands. *Geotech. Test. J.*, 29(6):507–516.
- Cho, G.-C., Dodds, J., and Santamarina, J. C. (2006). Particle shape effects on packing density, stiffness, and strength: Natural and crushed sands. *J. Geotech. Geoenviron.*, 132(5):591–602.
- Deiminiat, A. and Li, L. (2022). Experimental study on the reliability of scaling down techniques used in direct shear tests to determine the shear strength of rockfill and waste rocks. *CivilEng*, 3(1):35–50.
- Deiminiat, A., Li, L., Zeng, F., Pabst, T., Chiasson, P., and Chapuis, R. (2020). Determination of the shear strength of rockfill from small-scale laboratory shear tests: A critical review. *Adv. Civ. Eng.*, 2020:1–18.
- Deng, Y., Yilmaz, Y., Gokce, A., and Chang, C. (2021). Influence of particle size on the drained shear behavior of a dense fluvial sand. *Acta Geotech.*, 16(7):2071–2088.
- Dubois, F., Acary, V., and Jean, M. (2018). The contact dynamics method: A nonsmooth story. *C. R. Mécanique*, 346(3):247–262.
- Dubois, F., Jean, M., and et al (2023). LMG90 wiki page. [https://git-xen.lmgc.univ-montp2.fr/lmgc90/lmgc90\\_user/wikis/home](https://git-xen.lmgc.univ-montp2.fr/lmgc90/lmgc90_user/wikis/home). [Online; accessed 15-Mar-2023].
- Dubois, F., Jean, M., Renouf, M., Mozul, R., Martin, A., and Bagnéris, M. (2011). LMG90. In *10e colloque national en calcul des structures*. 10e colloque national en calcul des structures.
- Estrada, N., Azéma, E., Radjai, F., and Taboada, A. (2011). Identification of rolling resistance as a shape parameter in sheared granular media. *Phys. Rev. E*, 84(1).
- Frossard, E., Ovalle, C., Dano, C., Hicher, P.-Y., Maiolino, S., and Hu, W. (2013). Size effects due to grain crushing in rockfills shear strength. In *be published in 18th International Conference for Soil Mechanics and Geotechnical Engineering*.
- GDR-MiDi (2004). On dense granular flows. *Eur. Phys. J. E*, 14:341–365.
- Hardin, B. O. (1985). Crushing of soil particles. *J. Geotech. Eng.*, 111(10):1177–1192.
- Hidalgo, R. C., Zuriguel, I., Maza, D., and Pagonabarraga, I. (2009). Role of particle shape on the stress propagation in granular packings. *Phys. Rev. Lett.*, 103(11).
- Hu, W., Dano, C., Hicher, P.-Y., Le Touzo, J.-Y., Derx, F., and Merliot, E. (2011). Effect of sample size on the behavior of granular materials. *Geotech. Test. J.*, 34(3):186–197.
- Indraratna, B., Ionescu, D., and Christie, H. (1998). Shear behavior of railway ballast based on large-scale triaxial tests. *J. geotechn. geoenviron.*, 124(5):439–449.
- Jean, M. and Moreau, J. J. (1992). Unilaterality and dry friction in the dynamics of rigid body collections. In *1st Contact Mechanics International Symposium*, pages 31–48. 1st Contact Mechanics International Symposium.
- Jullien, R., Pavlovitch, A., and Meakin, P. (1992). Random packings of spheres built with sequential models. *J. Phys. A Math. Theor.*, 25(15).
- Kanzaki, T., Acevedo, M., Zuriguel, I., Pagonabarraga, I., Maza, D., and Hidalgo, R. (2011). Stress distribution of faceted particles in a silo after its partial discharge. *Eur. Phys. J. E*, 34(12):1–8.
- Kawamoto, R., Andò, E., Viggiani, G., and Andrade, J. E. (2018). All you need is shape: Predicting shear banding in sand with ls-dem. *J. Mech. Phys. Solids*, 111:375–392.
- Lade, P. V., Yamamuro, J. A., and Bopp, P. A. (1996). Significance of particle crushing in granular materials. *J. Geotech. Eng.*, 122(4):309–316.
- Li, G., Ovalle, C., Dano, C., and Hicher, P.-Y. (2013). Influence of grain size distribution on critical state of granular materials. In *Constitutive modeling of geomaterials*, pages 207–210. Springer.
- Linero, S., Azéma, E., Estrada, N., Fityus, S., Simmons, J., and Lizcano, A. (2019). Impact of grading on steady-state strength. *Geotech. Lett.*, 9(4):328–333.

- Linero, S., Fityus, S., Simmons, J., Lizcano, A., and Cassidy, J. (2017). Trends in the evolution of particle morphology with size in colluvial deposits overlying channel iron deposits. In *EPJ Web of Conferences*, volume 140. EPJ Web of Conferences.
- Linero, S., Palma, C., and Apablaza, R. (2007). Geotechnical characterisation of waste material in very high dumps with large scale triaxial testing. In *Proceedings of the 2007 International Symposium on Rock Slope Stability in Open Pit Mining and Civil Engineering*, pages 59–75. Australian Centre for Geomechanics.
- Liu, Y., Guillard, F., Marks, B., Rognon, P., and Einav, I. (2022). The perpetual shearing of granular soils under low stresses using the stadium shear device. *Open Geomechanics*, 3:1–19.
- Marachi, N., Chan, C., and Seed, H. (1972). Evaluation of properties of rockfill materials. *J. Soil Mech. Found. Div.*, 98(1):95–114.
- Marsal, R. (1967). Large scale testing of rockfill materials. *J. Soil Mech. Found. Div.*, 93(2):27–43.
- Matsuoka, H., Liu, S., Sun, D., and Nishikata, U. (2001). Development of a new in-situ direct shear test. *Geotech. Test. J.*, 24(1):92–102.
- Matsushima, T. and Chang, C. S. (2011). Quantitative evaluation of the effect of irregularly shaped particles in sheared granular assemblies. *Granul. Matter*, 13(3):269–276.
- Moreau, J. J. (1988). Unilateral contact and dry friction in finite freedom dynamics. In *Nonsmooth mechanics and Applications*, pages 1–82. Springer.
- Muir Wood, D. and Maeda, K. (2008). Changing grading of soil: Effect on critical states. *Acta Geotech.*, 3:3–14.
- Nguyen, D. H., Azéma, E., Sornay, p., and Radjai, F. (2015). Effects of shape and size polydispersity on strength properties of granular materials. *Phys. Rev. E*, 91.
- Nicot, F., Hadda, N., Guessasma, M., Fortin, J., and Millet, O. (2013). On the definition of the stress tensor in granular media. *Int. J. Solids Struct.*, 50(14-15):2508–2517.
- Nouguier-Lehon, C. (2010). Effect of the grain elongation on the behaviour of granular materials in biaxial compression. *C. R. Mécanique*, 338(10):587–595. Micromechanics of granular materials.
- Ovalle, C. and Dano, C. (2020). Effects of particle size–strength and size–shape correlations on parallel grading scaling. *Geotech. Lett.*, 10(2):191–197.
- Ovalle, C., Dano, C., Hicher, P.-Y., and Cisternas, M. (2015). Experimental framework for evaluating the mechanical behavior of dry and wet crushable granular materials based on the particle breakage ratio. *Can. Geotech. J.*, 52(5):587–598.
- Ovalle, C., Frossard, E., Dano, C., Hu, W., Maiolino, S., and Hicher, P. Y. (2014). The effect of size on the strength of coarse rock aggregates and large rockfill samples through experimental data. *Acta Mech.*, 225:2199–2216.
- Ovalle, C., Linero, S., Dano, C., Bard, E., Hicher, P.-Y., and Osses, R. (2020). Data compilation from large drained compression triaxial tests on coarse crushable rockfill materials. *J. Geotech. Geoenviron.*, 146.
- Radjai, F. and Richefeu, V. (2009). Contact dynamics as a nonsmooth discrete element method. *Mech. Mater.*, 41(6):715–728. Advances in the Dynamics of Granular Materials.
- Rothenburg, L. and Bathurst, R. J. (1989). Analytical study of induced anisotropy in idealized granular materials. *Geotechnique*, 39(4):601–614.
- Saussine, G., Cholet, C., Gautier, P., Dubois, F., Bohatier, C., and Moreau, J. (2006). Modelling ballast behaviour under dynamic loading. part 1: A 2d polygonal discrete element method approach. *Comput. Methods Appl. Mech. Eng.*, 195(19):2841–2859.
- Schuhmacher, P. (2016). *Rhéologie des écoulements granulaires : variables internes et effets d'échelle*. Thesis, Université Montpellier.
- Varadarajan, A., Sharma, K., Venkatachalam, K., and Gupta, A. (2003). Testing and modeling two rockfill materials. *J. Geotech. Geoenviron.*, 129(3):206–218.
- Verdugo, R. and de La Hoz, K. (2007). Strength and stiffness of coarse granular soils. In *Soil stress-strain behavior: Measurement, modeling and analysis*, pages 243–252. Springer.
- Visscher, W. M. and Bolsterli, M. (1972). Random packing of equal and unequal spheres in two and three dimensions. *Nature*, 239:504–507.
- Voivret, C., Radjai, F., Delenne, J. Y., and El Youssofi, M. S. (2007a). Space-filling properties of polydisperse granular media. *Phys. Rev. E*, 76.
- Voivret, C., Radjai, F., Delenne, J.-Y., and El Youssofi, M. S. (2007b). Space-filling properties of polydisperse granular media. *Phys. Rev. E*, 76(2).
- Wadell, H. (1933). Sphericity and roundness of rock particles. *The Journal of Geology*, 41(3):310–331.
- Xiao, Y., Liu, H., Chen, Y., and Zhang, W. (2014). Particle size effects in granular soils under true triaxial conditions. *Géotechnique*, 64(8):667–672.
- Xiao, Y., Long, L., Matthew Evans, T., Zhou, H., Liu, H., and Stuedlein, A. W. (2019). Effect of particle shape on stress-dilatancy responses of medium-dense sands. *J. Geotech. Geoenviron.*, 145.
- Yang, J. and Luo, X. D. (2018). The critical state friction angle of granular materials: does it depend on grading? *Acta Geotech.*, 13:535–547.
- Youd, T. L., Nichols, D., Helley, E., and LaJoie, K. (1973). Liquefaction potential of unconsolidated sediments in the southern san francisco bay region, california. Technical report, US Geological Survey.
- Zeller, J. and Wullimann, R. (1957). The shear strength of the shell materials for the go-schenenalp dam, switzerland. In *4th International Conference on Soil Mechanics and Foundation Engineering*, volume 2, pages 399–415.
- Zheng, J. and Hryciw, R. D. (2016). Index void ratios of sands from their intrinsic properties. *J. Geotech. Geoenviron.*, 142(12).

Manuscript received 3rd March 2023, revised 5th June 2023, accepted 5th July 2023.